Analysis of the correlation between n-value and critical current in bent multifilamentary Bi2223 composite tape based on a damage evolution model

Ochiai, S; Okuda, H; Fujimoto, M; Shin, J-K; Sugano, M; Hojo, M; Osamura, K; Oh, S S; Ha, D W

Analysis of Correlation between *n*-value and Critical Current in Bent Multifilamentary Bi2223 Composite Tape Based on Damage Evolution Model

S. Ochiai[a,*], H. Okuda[a], M. Fujimoto[a], J.-K. Shin[a], M. Sugano[b], M. Hojo[a], K. Osamura[c], S. S. Oh[d] and D. W. Ha[d]

[a] Graduate School of Engineering, Kyoto University, Yoshida, Sakyo-ku, Kyoto 606-8501, Japan.
[b] High Energy Accelerator Research Organization (KEK), Cryogenics Science Center, J-PARC Center, 203-1 Shirakata, Tokai-Mura, Naka-gun, Ibaraki 319-1106, Japan.
[c] Research Institute for Applied Sciences, Sakyo-ku, Kyoto 606-8202, Japan.
[d] Korea Electrotechnology Research Institute, 28-1 Sungju-Dong, Changwon 641-120, Korea

Abstract

The change in *n*-value and critical current with bending strain and the relation of *n*-value to critical current of bent-damaged Bi2223 composite tape were studied experimentally and analytically. The *n*-value of the bent-damaged Bi2223 filamentary composite tape decreased rather slightly with increasing bending strain and with decreasing critical current, in comparison with that of tension-damaged tape. To describe the experimental result of bent-damaged tape above, a damage evolution model was applied, in which the steep tensile strain-variation in the thickness direction, shape of the core in which superconducting filaments are bundled into and the damage strain parameters obtained from the analysis of the tensile stress-strain curve were incorporated. The measured change in *n*-value and critical current with bending strain and the relation of *n*-value to critical current under applied bending strain were described satisfactorily by the present approach.

PACS codes: 74.25 Sv; 74.25 Ld
Keywords: Bi2223 composite tape; Critical current; *n*-value; Bending strain; Damage evolution

*Corresponding author.
Prof. Shojiro Ochiai
Postal address: Department of Materials Science and Engineering, Graduate School of Engineering, Kyoto University, Yoshida, Sakyo-ku, Kyoto 606-8501, Japan
Phone: +81 75 753 4834
Fax: +81 75 753 4841
E-mail address: shojiro.ochiai@materials.mbox.media.kyoto-u.ac.jp

1. Introduction

$(Bi,Pb)_2Sr_2Ca_2Cu_3O_{10+\delta}$ (Bi2223) composite superconductor tapes have been developed for high in-field applications, such as magnets and motors [1]. They are subjected to stresses such as (a) residual stresses arising from the mismatch of the coefficient of thermal expansion among the constituents, (b) tensile and bending stresses during winding to make coils and (c) electro-magnetic (Lorentz) force in operation [2-4]. The brittle Bi2223 filaments that transport superconducting current are damaged when the subjected stresses are high. Accordingly, it is needed to clarify the influence of damage evolution on the superconducting property for reliability and safe design. Until now, it has been revealed that, once the applied strain exceeds the irreversible strain at which damage initiates, the critical current never returns to the original value even when the applied strain is released, while it returns reversibly when the applied strain is lower than the irreversible strain [1-26]. Such a feature has been observed commonly under tensile and bending strain-application. On the other hand, the damage initiation and evolution behavior under tensile strain is different from that under bending strain, as follows.

Under application of tensile strain (ε_T), the weaker filaments within the gauge length are cracked in the early stage, and then the stress concentration arising from the cracked filaments causes collective cracks (cracks composed of successively cracked filaments in a transverse cross-section [7, 27]), reducing critical current seriously. Under application of bending strain (ε_B), filament-cracking is caused also mainly by the tensile strain in the sample length direction but its extent is dependent on location in sample thickness direction [14-16, 24-26]. The strain of Bi2223 filament ε_{Bi2223} in the sample length direction, induced by applied bending strain, varies steeply along the thickness direction; it is equal to the residual strain (ε_r) at the neutral axis and it increases and decreases with distance from the neutral axis in the tensile- and compressive sides, respectively. The filaments at the positions apart from the neutral axis are cracked severely, while those at the position near the neutral axis are less cracked.

Due to the difference in damage evolution between tensile (ε_T)- and bending (ε_B)-strain application, it is expected that the change in critical current and n-value with increasing applied strain and also the correlation of n-value to critical current are different. The aims of the present work are (i) to assure experimentally these expected features and (ii) to describe the experimental results under bending strain by modeling analysis from a viewpoint of damage evolution.

2. Experimental procedure

2.1 Sample

The multifilamentary Bi2223/Ag/Ag alloy composite tape, fabricated at Korea Electrotechnology Research Institute (KERI), was used as the sample. It contained 55 Bi2223 filaments. The thickness (t) and width (W) of the sample were 0.23 mm and 4.1 mm, respectively. The residual strain ε_r of Bi2223 filaments in this sample at room temperature has been estimated to be –0.12 % with an X-ray diffraction method [15]. Also it has been shown that, under applied bending strain ε_B up to 0.83 %, damage occurs only in the tensile side [15, 25].

2.2. Procedure for measurement of critical current and *n*-value

As the damage behavior and hence critical current and n-value differ among test specimens [24, 25], many specimens are needed to extract the feature of the relation of n-value to critical current (I_c). In the present work, we used the test specimens with a configuration shown in Fig.1. Seven voltage probes were attached in a step of 1 cm in the test specimens with a length 6 cm. The V (voltage)-I (current) curve was measured for 6 sections (S1 to S6 in Fig.1) with a length L=1 cm. Two test-specimens were used in experiment. Thus for totally 12 sections, I_c- and n-values were measured at each bending strain ε_B and the results were averaged for analysis.

Bending strain ε_B was given at room temperature by pressing the test specimens with the upper GFRP (Glass Fiber Reinforced Plastic) die to the lower one with the same curvature, similarly to the round robin test of VAMAS (Versailles project on advanced materials and standard)/TWA 16 (Technical working area 16, superconducting materials) [21]. Six pairs of dies with different curvatures were used and the specimens were bent by ε_B=0, 0.19, 0.39, 0.52, 0.67 and 0.83 %. The specimens bent at room temperature were cooled down to 77K, at which $V - I$ curves were measured in a self magnetic field. The V–I curve was approximated by

$$V=LE_c(I/I_c)^n \qquad (1)$$

where E_c(=1 μV/cm) is the electric filed criterion for critical current. n-value in Eq.(1) was estimated for the range of V/L=0.1 to 10 μV/cm.

Also the specimens shown in Fig.1 were pulled in tension at 77K and the V–I curves were measured at 77K for 12 sections. Due to the difference in damage behavior among sections, the strains of sections are different to each other but stress is common for all

sections. Due to this reason, stress is used instead of strain as a measure of applied mechanical condition. The tensile stress σ_T was given stepwise to test specimens up to 137 MPa. The I_c- and n-values under applied tensile stress were estimated in the same manner as those under applied bending strain.

3. Measured critical current- and *n*-values, and correlation of *n*-value to critical current

Figure 2 shows the change in (a) critical current I_c and (b) n-value with bending strain ε_B up to 0.83%. The decrease in n-value (b) with increasing ε_B is rather slight in comparison with that in critical current (a). Such a slight decrease in n-value with increasing ε_B has been reported also for the different supplier's Bi2223 composite tape [21]. Figure 3 shows the change in (a) critical current I_c and (b) n-value with tensile stress σ_T. The decrease in n-value (b) with increasing tensile stress as well as that in critical current (a) is large above 120 MPa.

Figure 4 shows the comparison of the relation of n-value to critical current I_c measured under bending strain with that measured under tensile stress. The data under bending strain at ε_B=1.0% (open circles), measured for the same sample with the same procedure as in the present work, were taken from our former work [24]. The following features are read. (i) In the range of I_c > 40 A, the decrease in n-value with decreasing I_c under bending strain is small in comparison with that under tensile stress. (ii) When I_c becomes lower than 40 A, the decrease in n-value with decreasing I_c under bending strain becomes very sharp. The reason for this could be attributed to the damage evolution in the compression side [24]. Otto et al. [12] reported that the buckling of the filaments occurs under compressive stress and the plural filaments are damaged at the same time by the buckling. At high bending strain such as ε_B=1.0% for the present sample, when compressive side is damaged in addition to tensile side, n-value decreases seriously due to the buckling fracture.

As shown above, under tensile stress, n-value decreases significantly with decreasing I_c. In contrast, the slight decrease in n-value with increasing ε_B up to 0.83 % and slight decrease in n-value with decreasing critical current up to ε_B=0.83 % are the features in the case of bending strain application. Such a feature could be described below, by modeling analysis.

4. Analysis of the experimental results by a damage evolution model under bending strain

4.1 Estimation of damage strain parameters $\varepsilon_{f,1}$ and $\varepsilon_{f,2}$ from tensile stress (σ_T) –strain (ε_T) curve at room temperature

In the present work, the specimens were bent at room temperature and were cooled down to 77 K at which critical current and *n*-value were measured. When the specimens are cooled to 77 K, compressive strain is added to the Bi2223 filaments in the current transport direction due to the higher coefficient of thermal expansion of metallic constituents of Ag and Ag alloy than that of Bi2223 filaments [13, 15, 17]. As the damage of filaments in the bent specimens is caused by the tensile strain in the current transport direction, the filaments have been damaged by the bending-induced tensile strain at room temperature. The additionally exerted compressive strain on filaments at 77 K due to cooling does not cause further damage. The damage of the filaments at room temperature is conserved at 77 K, and hence, the critical current at 77 K is determined by the damage at room temperature [15-17]. Due to this reason, the residual strain and the stress-strain curve at room temperature are used for analysis below.

As stated above, as bending strain was applied to specimens at room temperature, the damage was introduced at room temperature. Cracking of filaments is caused when the filament strain ε_{Bi2223} in the longitudinal direction reaches its fracture strain. The ε_{Bi2223} varies steeply in the sample thickness direction and hence the extent of damage is location-dependent, which is the cause of the slight decrease in *n*-value with decreasing I_c, as shown later in Subsection 4.4. In this subsection, we estimate two damage strain parameters from the tensile stress-strain curve at room temperature, for modeling the location-dependent damage extent under bending stain. One refers to the tensile strain at initiation of damage ($\varepsilon_{Bi2223}=\varepsilon_{f,1}$) and another to the tensile strain at which damage has occurred seriously ($\varepsilon_{Bi2223}=\varepsilon_{f,2}$). These parameters will be used in the modeling and calculation in the subsequent subsections.

It has been shown [5, 7, 13-16] that the tensile strain that causes cracking of the filaments is given by $\varepsilon_f-\varepsilon_r$ where ε_f is the tensile fracture strain of the bare Bi2223 filament and ε_r is the residual strain of the filaments in composite tape, arising during cooling down from heat-treatment- to room- temperature due to the difference in coefficient of thermal expansion among the constituents (Bi2223, Ag and Ag alloy) [13, 15, 17]. The residual strain ε_r of the present sample at room temperature has been estimated to be –0.12% (compressive strain) with an X-ray diffraction method [15].

Under applied tensile strain (stress), the cracking occurs first in the weakest filament with the lowest $\varepsilon_f - \varepsilon_r$ value. Regarding the ε_r (–0.12%) to be common for all

filaments and noting the lowest intrinsic fracture strain $\varepsilon_{f,1}$, we define the lowest $\varepsilon_f-\varepsilon_r$ value as $\varepsilon_{f,1}-\varepsilon_r$. This value corresponds to the irreversible strain under tension. Number of cracked filaments increases with increasing applied strain, leading to reduction in critical current. In the late stage, the surviving filaments that have high $\varepsilon_f-\varepsilon_r$ values in the cross-section in which filaments are most severely cracked, are also cracked, resulting in almost zero critical current. We note such a high $\varepsilon_f-\varepsilon_r$ value as $\varepsilon_{f,2}-\varepsilon_r$. The values of $\varepsilon_{f,1}-\varepsilon_r$ and $\varepsilon_{f,2}-\varepsilon_r$ can be estimated from the tensile stress - strain curve by using the procedure in our preceding work [17], as follows.

Figure 5(a) shows the measured tensile stress (σ_T)–strain (ε_T) curve of the sample at room temperature, which had been cooled down to 77K for pre-check of critical current and then had been warmed up to room temperature at KERI. The stress-strain curve was analyzed in our preceding work by using the residual strain (–0.12%) of Bi2223 filaments [15]. Silver is yielded in compression at $\varepsilon_T = 0\%$ and is yielded in tension at $\varepsilon_T = 0.05\%$. Ag alloy deforms elastically up to $\varepsilon_T = 0.12\%$, at which Ag alloy is yielded in tension. Thus, all constituents of Ag, Ag alloy and Bi2223 filaments deform elastically in the range of $0<\varepsilon_T<0.05\%$ (Stage I), Ag alloy and Bi2223 filaments deform elastically but Ag deforms plastically in the range of $0.05\%<\varepsilon_T<0.12\%$ (Stage II), and only Bi2223 filaments deform elastically in the range of $0.12\%<\varepsilon_T$ (Stage III). In Stage III, cracking of filaments initiates and the number of cracked filaments increase with increasing applied tensile strain. With further increasing applied tensile strain ($\varepsilon_T >$ 0.25 % in the present sample (Fig.5(a)), the sample deforms at nearly constant stress, where the loss of stress-bearing capacity due to multiple cracking of filaments (once-cracked filaments are continually cracked in other cross-sections) is balanced with the strain hardening-induced increase in stress carrying capacity of the Ag and Ag alloy [7, 15, 17].

The filament cracking initiates in advance of such a stress-constant stage [7, 14, 17]. The stress-strain range, covering the cracking- initiation and -evolution stages and part of multiple cracking stage, is shown with a rectangle (Fig.5(a)). In this strain range, the cracked filaments cause reduction in Young's modulus and hence cause reduction in slope of the stress-strain curve. The variation of the slope $d\sigma_T/d\varepsilon_T$ with strain ε_T in such a stress-strain range is shown in Fig.5(b). ε_T is expressed as $\varepsilon_T = \varepsilon_{Bi2223} - \varepsilon_r$. At $\varepsilon_T = 0$ %, the strain of the Bi2223 filaments ε_{Bi2223} is equal to ε_r (compressive and therefore negative [7, 13, 15, 17]). With increasing ε_T, ε_{Bi2223} becomes zero at $\varepsilon_T = -\varepsilon_r$ and becomes ε_f (fracture strain of bare filaments) at $\varepsilon_T = \varepsilon_f-\varepsilon_r$. Thus, $\varepsilon_{f,1}-\varepsilon_r$ (= the strain at initiation of filament cracking) can be estimated from the tensile strain ε_T at which the reduction in slope initiates. Here, it is noted that the strain hardening rate of the

plastically deforming Ag and Ag alloy decreases gradually with increasing strain, which is a common feature of ductile metals. The slight decrease in slope up to ε_T=0.21% in Fig.5(b) is attributed to this phenomenon [17]. Beyond ε_T=0.21%, the slope decreases sharply, due to the cracking of filaments. Thus, $\varepsilon_{f,1}-\varepsilon_r$ is estimated to be 0.21 %, as shown in Fig.5(b). $\varepsilon_{f,2}-\varepsilon_r$ (= the strain at which all filaments come to be cracked in a cross-section where cracking of filaments is most advanced) can be estimated from the tensile strain ε_T at which the slope reaches zero, respectively. Thus, $\varepsilon_{f,2}-\varepsilon_r$ is estimated to be 0.25 %, as shown in Fig.5(b). As ε_r is –0.12% in the present sample [15], $\varepsilon_{f,1}$ and $\varepsilon_{f,2}$ are estimated to be 0.09 % and 0.13 %, respectively.

From the results above, the following three regions can be distinguished, as shown in Fig.5(b): Region 0 (non-damaged region) with the ε_{Bi2223} range of $\varepsilon_{Bi2223} \le \varepsilon_{f,1}$, existing in the tensile strain range of $\varepsilon_T \le \varepsilon_{f,1}-\varepsilon_r$, Region 1 (partially damaged region where cracked and non-cracked filaments co-exist) with the ε_{Bi2223} range of $\varepsilon_{f,1} \le \varepsilon_{Bi2223} \le \varepsilon_{f,2}$, existing in the tensile strain range of $\varepsilon_{f,1}-\varepsilon_r \le \varepsilon_T \le \varepsilon_{f,2}-\varepsilon_r$, and Region 2 (seriously damaged region where multiple cracking of Bi2223 filaments occurs) with the ε_{Bi2223} range of $\varepsilon_{f,2} \le \varepsilon_{Bi2223}$, existing in the tensile strain range of $\varepsilon_{f,2}-\varepsilon_r \le \varepsilon_T$.

4.2 Formulation of the damage evolution in the core

The Bi2223 filamentary composite is composed of the sheath of Ag alloy and the core in which the filaments are bundled into Ag. Figure 6(a) shows the micrograph of the transverse cross-section of the sample, in which the thickness direction is three times magnified from the as-observed one as to show clearly the shape of the core. The boundary of the core is shown with a broken curve. Figure 6(b) shows the schematic representation of the geometry of the transverse cross-section. W_{core} and t are the width of the core and thickness of the sample, which have been measured to be 3.90 mm and 0.23 mm, respectively. The width and thickness directions of the composite tape are taken to be as x and y, respectively, and the center of the composite tape as x=y=0. The core boundary y_{core} (ABCDEFGHA) is expressed as a function of x with the following 9th order polynomials [25]. The length unit is millimeters.

$$\left.\begin{aligned}
&\text{CDE: } y_{core}=0.0660214-0.0405173x+1.03050x^2-4.05239x^3\\
&\qquad +8.94014x^4-12.6431x^5+11.3895x^6-6.22952x^7\\
&\qquad +1.87094x^8-0.235769x^9 \qquad \text{for } 0\le x\le 1.95\\
&\text{ABC: symmetry with EDC with respect to } x=0\\
&\text{AHGFE: symmetry with ABCDE with respect to } y=0
\end{aligned}\right\} \quad (2)$$

The maximum value of y_{core}, $y_{core,max}$, at B and D in Fig.6(b) was 0.101 mm. Under the application of bending strain ε_B, when ε_B reaches the irreversible bending strain $\varepsilon_{B,irr}$, damage of Bi2223 filaments takes place first at $y=y_{core,max}$. Beyond $\varepsilon_{B,irr}$, the damage front extends towards y=0 (neutral axis) with increasing ε_B, resulting in reduction in critical current. At a given ε_B($> \varepsilon_{B,irr}$), the bending strain-induced tensile strain varies largely along the sample thickness direction y and hence non-damaged-, partially damaged- and seriously damaged regions appear, as follows.

As noted in Subsection 2.1, the present sample is damaged only in the tensile side ($0<y$) within the bending strain range 0 ~ 0.83% [15, 25]. Under the application of bending strain ($\varepsilon_B \leq 0.83$ %), the relation among y-coordinate, bending strain ε_B, sample thickness t and the strain ε_{Bi2223} of the filaments in longitudinal direction under bending strain is expressed as [14, 16, 17]

$$\varepsilon_{Bi2223}=\varepsilon_B y/(t/2) + \varepsilon_r \qquad (3)$$

Though Eq.(3) is not rigid, it has been shown that, by using Eq.(3), experimental results of I_c-ε_B relation for many different fabrication route samples can be described successfully [14-17, 24-26]. Equation (3) is a useful tool practically.

ε_{Bi2223} increases with increasing y from ε_r (= –0.12%) at y=0 to $\varepsilon_B+\varepsilon_r$ at $y=t/2$. As has been shown in Subsection 4.1, Bi2223 filaments are cracked first at $\varepsilon_{Bi2223} = \varepsilon_{f,1}$ = 0.09 % and are cracked seriously at $\varepsilon_{Bi2223} = \varepsilon_{f,2}$ = 0.13 % under tensile strain. Noting the y-positions at $\varepsilon_{Bi2223} = \varepsilon_{f,1}$ and $\varepsilon_{f,2}$ as y_1 and y_2, respectively, we can obtain the y_1- and y_2-values for a given ε_B by substituting $\varepsilon_{Bi2223} = \varepsilon_{f,1}$ = 0.09 % and $\varepsilon_{Bi2223} = \varepsilon_{f,2}$ = 0.13 %, respectively, together with the sample thickness t = 0.23 mm and ε_r = –0.12 %, into Eq.(3), as schematically shown in Fig.6(c). The damage situation in the core in the transverse cross-section is shown in Fig.6(b).

The extent of damage in the core is dependent on y-position; the regions locating in $-y_{core,max} \leq y \leq y_1$, $y_1 \leq y \leq y_2$ and $y_2 \leq y \leq y_{core,max}$ are non-damaged, partially-damaged and seriously-damaged, respectively. Thus, under bending strain, Regions 0, 1 and 2, observed under tensile strain (Fig.5(b)), also appear, and are characterized as follows.

*In Region 0 (non-damaged region locating in $-y_{core,max} \leq y \leq y_1$), as the ε_{Bi2223} is lower than $\varepsilon_{f,1}$, all filaments transport current and critical current is retained.

*In Region 1 (partially-damaged region locating in $y_1 \leq y \leq y_2$), as ε_{Bi2223} is higher than $\varepsilon_{f,1}$ and lower than $\varepsilon_{f,2}$, cracked and non-cracked filaments co-exist and hence critical current is recued.

*In Region 2 (seriously-damaged region locating in $y_2 \leq y \leq y_{core,max}$), as ε_{Bi2223} is higher than $\varepsilon_{f,2}$, all filaments are cracked and critical current is almost zero.

It is noted that the bending strains $\varepsilon_{B,1}$ and $\varepsilon_{B,2}$, at which Regions 1 and 2 appear, are given by $(\varepsilon_{f,1}-\varepsilon_r)/\{y_{core,max}/(t/2)\}$ and $(\varepsilon_{f,2}-\varepsilon_r)/\{y_{core,max}/(t/2)\}$, respectively, from Eq.(3). Substituting $\varepsilon_{f,1}-\varepsilon_r = 0.21$ %, $\varepsilon_{f,2}-\varepsilon_r = 0.25$%, $t = 0.23$ mm and $y_{core,max} = 0.10$ mm into these relations, we have $\varepsilon_{B,1} = 0.24$ % and $\varepsilon_{B,2} = 0.28$ %. $\varepsilon_{B,1} = 0.24$ % corresponds to the irreversible bending strain $\varepsilon_{B,irr}$. Thus, only Region 0 exists in the bending strain range of $\varepsilon_B \leq \varepsilon_{B,1}(0.24\%)$, Regions 0 and 1 co-exist in the bending strain range of $\varepsilon_{B,1}(0.24\ \%) \leq \varepsilon_B \leq \varepsilon_{B,2}(0.28\ \%)$ and all Regions 0, 1 and 2 co-exists in the bending strain range of $\varepsilon_B \geq 0.28\ \%(\varepsilon_{B,2})$.

Noting the cross-sectional area of the core as S_{core} (=0.66 mm^2 [25]), the cross-sectional areas of Regions 0, 1 and 2 as ΔS_0, ΔS_1 and ΔS_2, respectively, the x-coordinates at the cross-points of y_{core} (Eq.(1)) with y_1 as $-x_1$ and x_1, and the x-coordinates at the cross-points of y_{core} with y_2 as $-x_2$ and x_2, as shown in Fig.6(b), we can calculate $\Delta S_0/S_{core}$, $\Delta S_1/S_{core}$ and $\Delta S_2/S_{core}$ by,

$$\Delta S_0 / S_{core} = 0.5 + \left\{ \int_{-W_{core}/2}^{-x_1} y_{core} dx + 2x_1 y_1 + \int_{x_1}^{W_{core}/2} y_{core} dx \right\} / S_{core} \quad (4)$$

$$\Delta S_1 / S_{core} = \left\{ \int_{-x1}^{-x2} (y_{core} - y_1) dx + 2x_2 (y_2 - y_1) + \int_{x_2}^{x_1} (y_{core} - y_1) dx \right\} / S_{core} \quad (5)$$

$$\Delta S_2 / S_{core} = \int_{-x2}^{x2} (y_{core} - y_2) dx / S_{core} \quad (6)$$

Figure 7(a) shows the tensile strain ε_{Bi2223} of filaments calculated by Eq.(3) as a function of the normalized y-position with respect to the half thickness of the sample, $y/(t/2)$, at a bending strain of ε_B=0.66 % as an example. As $\varepsilon_{f,1}$ and $\varepsilon_{f,2}$ were 0.09 % and 0.13 %, respectively, the corresponding $y_1/(t/2)$ and $y_2/(t/2)$ were 0.32 and 0.38, respectively. The $y_{core.max}/(t/2)$ was 0.88. Thus, at ε_B=0.66 %, Regions 0, 1 and 2 were in the range of $-0.88 \leq y/(t/2) \leq 0.32$, $0.32 \leq y/(t/2) \leq 0.38$ and $0.38 \leq y/(t/2) \leq 0.88$, respectively. The solid curve in Fig.7(b) shows the cumulative cross-sectional area S/S_{core} of the core integrated from $y/(t/2) = -y_{core,max}/(t/2) = -0.88$ to $y/(t/2)$ as a function of $y/(t/2)$. The S/S_{core} values at $y_1/(t/2) = 0.32$ and $y_2/(t/2) = 0.38$ were 0.71 and 0.75, respectively. The fractions of cross-sectional area of Region 0 ($\Delta S_0/S_{core}$=0.71), Region 1 ($\Delta S_1/S_{core}$=0.04) and Region 2 ($\Delta S_2/S_{core}$=0.25) in the specimen bent by ε_B=0.66 % are also shown in Fig.7(b). In this way, by using the $\varepsilon_{f,1}$- and $\varepsilon_{f,2}$- values obtained from the

tensile stress-strain curve, the area fraction of each Region is calculated when a bending strain is given.

Figure 8 shows the calculated change in fraction of cross-sectional area of Region 0 ($\Delta S_0/S_{core}$), Region 1 ($\Delta S_1/S_{core}$) and Region 2 ($\Delta S_2/S_{core}$) as a function of bending strain ε_B. In the bending strain range up to $\varepsilon_B = \varepsilon_{B,1}$ (= $\varepsilon_{B,irr}$ = 0.24 %) where filaments are not cracked, $\Delta S_0/S_{core}$ remains 1(unity). Only Region 0 exists. Region 1 appears at $\varepsilon_B = \varepsilon_{B,1}$ = 0.24 % and then Region 2 appears at $\varepsilon_B = \varepsilon_{B,2}$ =0.28 %. The calculation results in Fig.8 shows that the fraction of cross-sectional area of Region 1, $\Delta S_1/S_{core}$, is small, being less than 0.07, in the whole bending strain range calculated, while that of Region 2, $\Delta S_1/S_{core}$, increases with increasing ε_B and reaches around 0.30 at ε_B =0.83 %.

4.3 Estimation of current amount transported by each region

The core is composed of parallel circuit of Regions 0, 1 and 2. Noting the critical current and *n*-value of Region *i* (*i*=0, 1 and 2) as $I_{c,i}$ and n_i, respectively, we can express the total current *I* as

$$I = \sum_{i=0}^{2} I_{c,i}(\Delta S_i / S_{core})(V / LE_c)^{1/n_i} \qquad (7)$$

The current I_i transported by Region *i* is calculated by

$$I_i = I_{c,i}(\Delta S_i / S_{core})(V / LE_c)^{1/n_i} \qquad (8)$$

As the values of $\Delta S_0/S_{core}$, $\Delta S_1/S_{core}$ and $\Delta S_2/S_{core}$ at various bending strains have been obtained as shown in Fig.8, *V*–*I* curves of the specimen and of each region can be calculated with Eqs.(7) and (8) when the $I_{c,i}$- and n_i- values characterizing Region *i* are given. In this work, $I_{c,0}$ and n_0 for Region 0 were taken to be 70 A and 18 from the average critical current and average *n*-value measured at ε_B=0 %, respectively. For Region 1, half of the critical current of the non-damaged state was taken as $I_{c,1}$ (35 A). The corresponding *n*-value, n_1, was taken to be 6 from the measured *n*-I_c relation under tensile strain (Fig.4). For Region 2, $I_{c,2}$ and n_2 were taken to be 2.5 A and 2.9, respectively, from the lowest set of I_c and *n*-values measured under tensile stress (Fig.4).

Figure 9(a) shows the calculated current of Regions 0 (I_0), 1(I_1) and 2 (I_2) with increasing total current *I* at ε_B=0.66% as an example. All of I_0, I_1 and I_2 increased with total current *I* and hence with increasing voltage *V*. It is noted that, at any *I* (and *V*), the I_0 was far higher than I_1 and I_2. For instance, the critical current I_c (*I* at *E*=*L*/*V*=1 μV/cm) in this example was 51 A. The values of I_0, I_1 and I_2 at *E*=1 μV/cm were 49 A,

1.4 A and 0.6 A, respectively. In order to examine whether the same feature is found or not at any bending strain, the variations in I_0/I_c, I_1/I_c and I_2/I_c with bending strain ε_B were calculated. The result is shown in Fig.9(b). The I_0/I_c was higher than 0.95 in the whole bending strain range calculated. The reason for this is attributed to the following features. (i) In Region 1, the fraction of cross-sectional area ($\Delta S_1/S$core) is very small, being less than several percent of the total area of the core (Fig.8), and also the ability of current transportation, $I_{c,1}$, is low due to cracked filaments. Accordingly, the product $I_{c,1}\times(\Delta S_1/S_{core})$ is far smaller than $I_{c,0}(\Delta S_0/S_{core})$. (ii) In Region 2, the fraction of cross-sectional area ($\Delta S_2/S$core) increases largely in contrast to that of Region 1 (Fig.8) but its contribution to overall current is small since the ability of current transportation, $I_{c,2}$, is very low due to the severe damage of filaments and hence $I_{c,2}\times(\Delta S_2/S_{core})$ is far smaller than $I_{c,0}(\Delta S_0/S_{core})$.

In this way, current is transported almost by Region 0 despite the co-existence of Regions 0, 1 and 2. However, as shown below, the slight decrease in n-value with ε_B (Fig.2(b)) cannot be accounted for if the contribution of either or both of Regions 1 and 2 are neglected.

4.4 Comparison of the I_c–ε_B, n–ε_B and n–I_c relations obtained by the present modeling analysis with experimental results

In order to examine the influence of Regions 0, 1 and 2 on I_c and n-value, the following Models were used.

*Model 0+1+2: All Regions 0, 1 and 2 were incorporated in calculation of Eq.(7). The calculation results by this model reflect the superimposed influences of all Regions. In order to distinguish the influence of each Region on I_c- and n-values, the following Models were additionally used.

*Model 0: As shown in Fig.9(a), the currents at $E = V/L$ = 0.1, 1 and 10 μV/cm are determined mostly by Region 0. Based on this result, as a first approximation, the contribution only of Region 0 was calculated by neglecting the contribution of Regions 1 and 2. In this model, $I_{c,1}$ and $I_{c,2}$ were set to be zero in calculation of Eq.(7).

*Model 0+1: In order to detect the influence of Region 1 on the result of Model 0, the contribution of Region 2 was neglected by setting $I_{c,2}$ =0 in calculation of Eq.(7).

Model 0+2: In order to detect the influence of Region 2 on the result of Model 0, the contribution of Region 1 was neglected by setting $I_{c,1}$ =0 in calculation of Eq.(7).

Substituting the values of $I_{c,i}$ and n_i (i=1,2 and 3) stated above for each model and the values of $\Delta S_i/S_{core}$ at each bending strain ε_B (Fig.8) into Eq.(7), V–I curve at each bending strain was calculated, from which I_c and n-value at each bending strain were

obtained with the same criteria as in experiment. The calculated I_c–ε_B relation, n–ε_B relation and correlation of n-value to I_c are shown in Fig.10 where the experimental results (average I_c and n-value at each bending strain) are also shown for comparison. The following features are read from Fig.10.

(i) The experimental result on change in I_c values with ε_B is described satisfactorily by all Models (Fig.10(a)). This result is attributed to the significant contribution of Region 0 which transports current more than around 95 % of total current at any ε_B (Fig.9(b)). The contributions of Regions 1 and 2 to I_c-values were minor, due to small cross-sectional area of Region 1 and due to almost lost superconductivity of Region 2.

(ii) The experimental result on change in n-value with ε_B (Fig.10(b)) and on n-I_c relation (Fig.10(c)) cannot be described by Model 0 that leads to no change in n-value. Model 0 is useful for description of change in I_c with ε_B due to the reason mentioned in (i) above but not for description of damage-induced change in n-value.

(iii) Model 0+1 describes the slight decrease in n-value in relatively high I_c range (low ε_B range), where the extent of damage is low and only Region 1 exists. In the narrow ε_B range (0~0.3 % in which irreversible bending strain $\varepsilon_{B,irr}$=0.24 % is included), this model is useful for description of n-value, but not for higher ε_B range where Region 2 appears. It is noted that, though Region 1 transports only small portion (less than 4%) of the current (Fig.9(b)), it acts to reduce n-value (Fig.10(b,c)). The slight increase in n-value with increasing ε_B in this model is attributed to the decrease in $\Delta S_1/S_{core}$ at high ε_B range (Fig.8).

(iv) The calculation result of Model 0+2 shows that, while Region 2 transports current very little (Fig.9(b)), it acts to reduce n-value as well as Region 1 (Fig.10(b,c)). Model 0+2 describes the trend of decrease in n-value with ε_B in the relatively low I_c range (high ε_B range) but cannot describe the decrease in n-value in low ε_B range below $\varepsilon_{B,2}$ (0.28%) and also in the ε_B range just beyond $\varepsilon_{B,2}$, for instance at ε_B=0.34%. Also, the n-value calculated by this model is slightly higher than the experimental results in the whole range of ε_B. In this way, both Model 0+1 and Model 0+2 cannot fully describe the change in n-value with ε_B and n-I_c relation.

(v) Model 0+1+2 describes satisfactorily the decrease in n-value with ε_B in the whole ε_B range investigated (Fig.10(a,b)) and the slight decrease in n-value with decreasing I_c (Fig.10(c)). This means that superimposed influences of both Region 1 and Region 2 contribute to the damage-induced decrease in n-value.

In the present work, a model composed of three regions (Regions 0, 1 and 2) was used as a first step for description of I_c-ε_B, n-ε_B and n-I_c relations of bent-damaged

Bi2223 tape. The approach was rough but could describe the experimental results satisfactorily. When modified as to include more regions with different extent of damage, it could be refined, and could be a useful tool for prediction especially of n-ε_B and n –I_c relations from the tensile data (tensile stress- strain curve, and I_c- and n-values measured under tensile strain).

4. Conclusions

(1) The n-value of the bent-damaged Bi2223 filamentary composite tape decreased rather slightly with increasing bending strain and with decreasing critical current, in comparison with that of tension-damaged tape.
(2) To describe the experimental result above, a damage evolution model, which combines the steep tensile strain-variation along the thickness direction, shape of the core and the damage strain parameters obtained by the analysis of the tensile stress-strain curve, was proposed.
(3) The measured change in n-value and critical current with bending strain and the relation of n-value to critical current were described satisfactorily by the present approach.
(4) While the current is changed mainly by the decrease in cross-sectional area of the non-damaged region, the n-value is changed by co-existent non-damaged-, partially damaged- and seriously damaged regions.

Acknowledgements

The authors wish to express their gratitude to The Ministry of Education, Culture, Sports, Science, and Technology, Japan for the grant-in-aid (no. 22360281).

References

[1] Kagiyama T, Yamazaki K, Kikuchi M, Yamade S, Nakashima T, Kobayashi S, Hayashi K, Sato K, Shimoyama J, Inoue M, Higashikawa K, Kiss T, Kitaguchi H and Kumakura H 2011 *IOP Conf. Series: Mater. Sci. Eng.* **18** 152001.
[2] Savvides N; Herrmann J, Reilly D, Muller K-H, Darmann F, McCaughey G, Zhao R and Apperly M 1998 *Physica C* **306** 129-35.
[3] Vase P, Flükiger R, Leghissa M and Glowacki B 2000 *Supercond. Sci. Technol*. **13** R71-84.

[4] Kitaguchi H, Itoh K, Kumakura H, Takeuchi T, Togano K and Wada H 2001 *IEEE Trans. Appl. Supercond*. **11** 3058-61.

[5] Passerini R, Dhalle' M, Giannini E, Witz G, Seeber B and Flükiger R 2002 *Physica C* **371** 173-84.

[6] Weijers H W, Schwartz J and ten Haken B 2002 *Physica C* **372-376** 1364-7.

[7] Ochiai S, Nagai T, Okuda H, Oh S S, Hojo M, Tanaka M, Sugano M and Osamura K 2003 *Supercond. Sci. Technol.* **16** 988-94.

[8] Shin H S and Katagiri K 2003 *Supercond. Sci. Technol.* **16** 1012-8.

[9] Katagiri K, Shin H S, Kasaba K, Tsukinokizawa T, Hiroi K, Kuroda T, Itoh K and Wada H 2003 *Supercond. Sci. Technol.* **16** 995-9.

[10] Hojo M, Nakamura M, Matsuoka T, Tanaka M, Ochiai S, Sugano M and Osamura K 2003 *Supercond. Sci. Technol.* **16** 1043-51.

[11] van der Laan D C, van Eck H J N, ten Haken B, ten Kate H H J and Schwartz J 2003 *IEEE Trans. Appl. Supercond.* **13** 3534-9.

[12] Otto A, Harley E J and Marson R 2005 *Supercond. Sci. Technol.* **18** S308-12.

[13] Ochiai S, Rokkaku H, Morishita K, Shin J K, Iwamoto S, Okuda H, Hojo M, Osamura K, Sato M, Otto A, Harley E J and Malozemoff A 2007 *Supercond. Sci. Technol.* **20** 202-10.

[14] Ochiai S, Matsuoka T, Shin J K, Okuda H, Sugano M, Mojo M and Osamura K 2007 *Supercond. Sci. Technol.* **20** 1076-83.

[15] Ochiai S, Shin J K, Iwamoto S, Okuda H, Oh S S, Ha D W and Sato M 2008 *J. Appl. Phys.* **103** 123911.

[16] Ochiai S, Shin J K, Okuda H, Sugano M, Hojo M, Osamura K, Kuroda T, Itoh K and Wada H 2008 *Supercond. Sci. Technol.* **21** 054002.

[17] Ochiai S, Okuda H, Sugano M, Hojo M and Osamura K 2010 *J. Appl. Phys.* **107** 083904.

[18] Larbalestier D C, Cai X Y, Feng Y, Edelman H, Umezawa A, Riley Jr. G N and Carter W L 1994 *Physica C* **221** 299-303.

[19] Passi J, Kalliohaka T, Korpela A, Söderlund L, Herman P F, Kvitkovic J and Majoros M 1999 *IEEE Trans. Appl. Supercond.* **9** 1598-601.

[20] Wang Y, Xiao L, Lin L, Xu X, Lu Y and Teng Y 2003 *Cryogenics* **43** 71-7.

[21] Kuroda T, Itoh K, Katagiri K, Goldacker W, Hsessler W, ten Haken B, Kiuchi M, Noto N, Ochiai S, Otabe S, Shin H S, Sosnowski J, Weijers H, Wada H and Kumakura K 2005 *Physica C* **425** 111-20.

[22] Wang Y, Dai S, Zhao X, Xiao L, Lin L and Hui D 2006 *Supercond. Sci. Technol.* **19** 1278-81.

[23] Mbaruku A L and Schwarz J 2007 *J. Appl. Phys.* **101** 073913.

[24] Ochiai S, Fujimoto M, Okuda H, Oh S S and Ha D W 2009 *J. Appl. Phys.* **105** 06912.

[25] Ochiai S, Fujimoto M, Shin J K, Okuda H, Oh S S and Ha D W 2009 *J. Appl. Phys.* **106** 103916.

[26] Ochiai S, Okuda H, Fujimoto M, Shin J K, Oh S S and Ha D W 2011 *Physica C* **471** 1114-8.

[27] Miyoshi Y, Van Lanen E P A, Dhallé M M and Nijhuits N 2009 *Supercond. Sci. Technol.* **22** 085009.

Figure Captions

Fig.1 Schematic representation of the test specimen, constituting of 6 sections (S1 to S6) with a length L=1 cm. 1 to 7 show the positions of the voltage probes. Critical current and n-value were measured for each section.

Fig.2 Change in (a) critical current I_c and (b) n-value with bending strain ε_B. In this experiment, bending strain ε_B was given at room temperature and bent specimen was cooled down to 77 K at which I_c- and n-values were measured.

Fig.3 Change in (a) critical current I_c and (b) n-value with tensile stress σ_T. In this experiment, tensile stress σ_T was given at 77 K and I_c- and n-values were subsequently measured at 77 K.

Fig.4 Comparison of the relation of n-value to critical current I_c measured under bending strain with that measured under tensile stress, where the data under bending strain ε_B=0~0.83% and the data under tensile stress were taken from Figs.2 and 3, respectively. The data under bending strain at ε_B=1.0%, measured for the same sample with the same procedure as in the present work, were taken from our former work [24].

Fig.5 Tensile stress-strain behavior of the composite tape at room temperature. (a) shows the tensile stress(σ_T)–strain(ε_T) curve at ε_T=0 ~ 0.3%. The curve and the strains at yielding of Ag (0.05%) and Ag alloy (0.12%) were taken from our preceding work [14]. Stage I, Stage II and Stage III refer to the deformation stages where Ag, Ag alloy and Bi2223 filaments deform elastically, Ag alloy and Bi2223 filaments deform elastically but Ag deforms plastically, and only Bi2223 filaments deform elastically, respectively. Damage (cracking of filaments) initiates and evolutes in the range surrounded by the rectangle in Stage III. (b) shows the change in slope σ_T/ε_T with tensile strain ε_T, obtained from the stress-strain curve in the range surrounded by the rectangle in (a), and the estimated values of $\varepsilon_{f,1}$–ε_r, $\varepsilon_{f,2}$–ε_r, $\varepsilon_{f,1}$ and $\varepsilon_{f,2}$. Region 0, Region II and Region III refer to the non-damaged, partially damaged and seriously damaged regions, respectively.

Fig.6 Damage evolution in the core. (a) shows the optical micrograph, in which the thickness direction is 3 times magnified from the as-observed one. The scales (200 μm and 600 μm) are given in actual length. The broken curve shows the boundary of the core in which Bi2223 filaments are bundled into. (b) Schematic representation of the

shape of the core. (c) Schematic representation of the relation of y to the tensile strain ε_{Bi2223} of Bi2223 filaments in composite tape. In (b) and (c), y_1 and y_2 refer to the y-coordinates at $\varepsilon_{Bi2223}=\varepsilon_{f,1}$ and $\varepsilon_{f,2}$, respectively. Region 0 ($-y_{core,max} < y < y_1$), Region 1 ($y_1 < y < y_2$) and Region 2 ($y_2 < y < y_{core,max}$) refer to the non-damaged-, partially damaged- and seriously damaged- regions in the core, respectively.

Fig.7 (a)Strain ε_{Bi2223} of Bi2223 filaments in the composite tape as a function of y-position normalized with respect to $t/2$, $y/(t/2)$, and the ranges of Regions 0, 1 and 2, in the specimen bent by ε_B=0.66 %, where $y/(t/2)$ = 0, $y_1/(t/2)$ and $y_2/(t/2)$ refer to the normalized y-position at $\varepsilon_{Bi2223} = \varepsilon_r$(–0.12%), $\varepsilon_{f,1}$(0.09 %) and $\varepsilon_{f,2}$ (0.13 %), respectively. (b)Cumulative cross-sectional area S/S_{core} of the core integrated from $y/(t/2) = -y_{core,max}/(t/2)$ = –0.88 to $y/(t/2)$ as a function of $y/(t/2)$ and the fractions of the cross-sectional area of Regions 0($\Delta S_0/S_{core}$), Region 1($\Delta S_1/S_{core}$) and Region 2($\Delta S_2/S_{core}$) in the specimen bent by ε_B=0.66 %.

Fig.8 Change in fraction of cross-sectional area of Region 0 ($\Delta S_0/S_{core}$), Region 1 ($\Delta S_1/S_{core}$) and Region 2 ($\Delta S_2/S_{core}$) with increasing bending strain ε_B.

Fig.9 (a) Calculated current of Region 0 (I_0), Region 1 (I_1) and Region 2 (I_2) with increasing total current I at ε_B = 0.66 % as an example. (b) Calculated variation in I_0/I_c, I_0/I_c and I_2/I_c with bending strain ε_B.

Fig.10 Comparison of the calculated (a) I_c–ε_B, (b) n–ε_B and (c) n–I_c relations by Model 0, Model 0+1, Model 0+2 and Model 0+1+2 with experimental results.

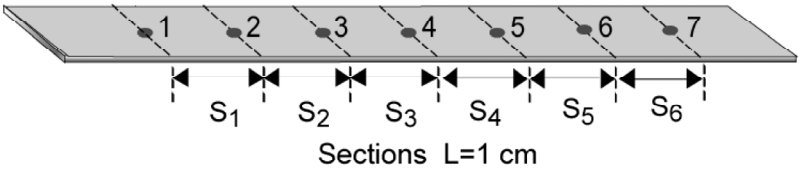

Fig.1

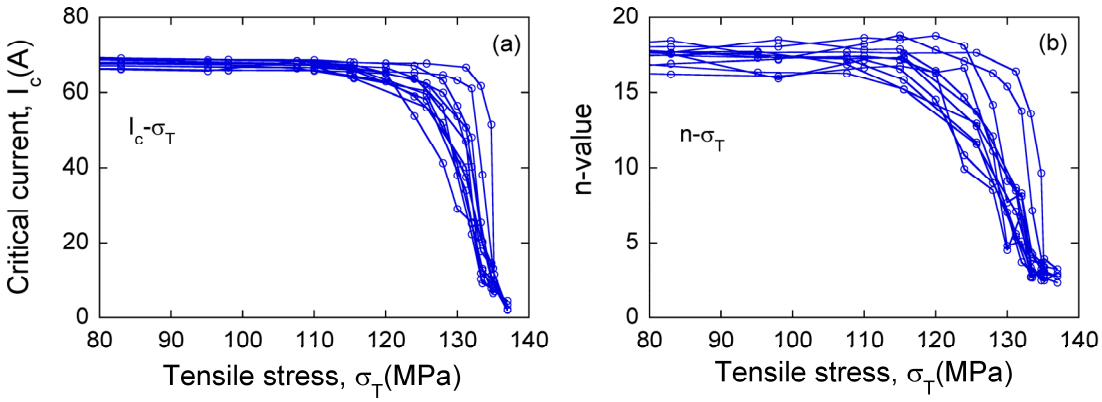

Fig.2

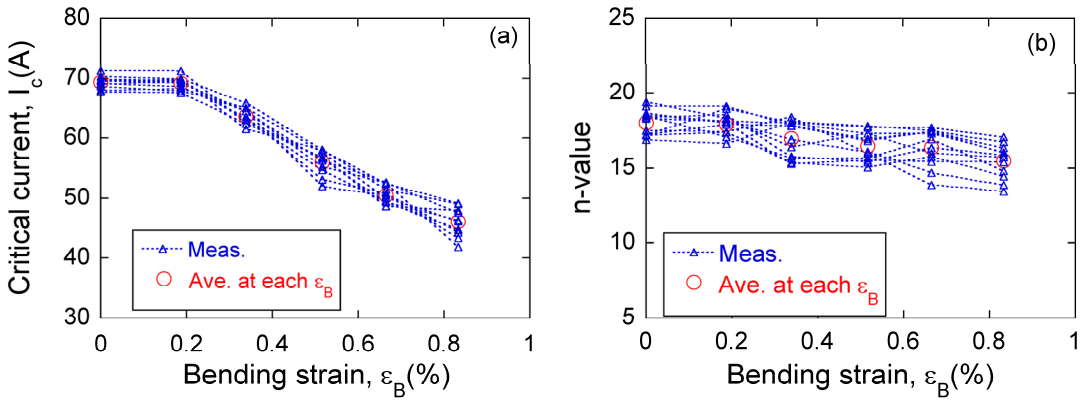

Fig.3

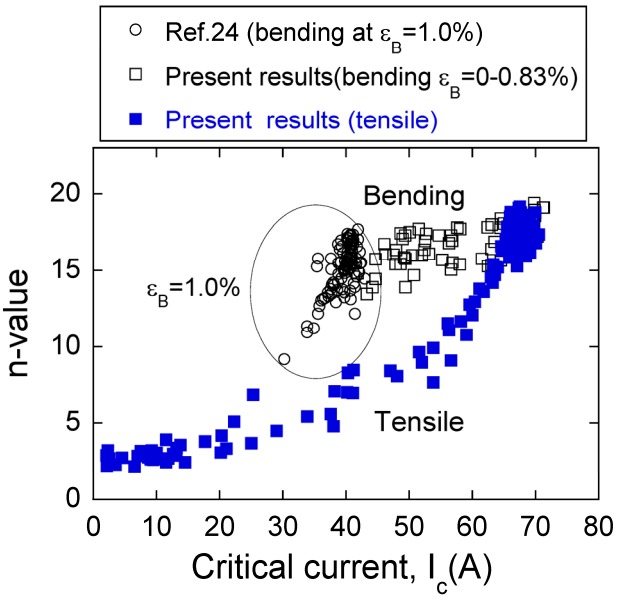

Fig.4

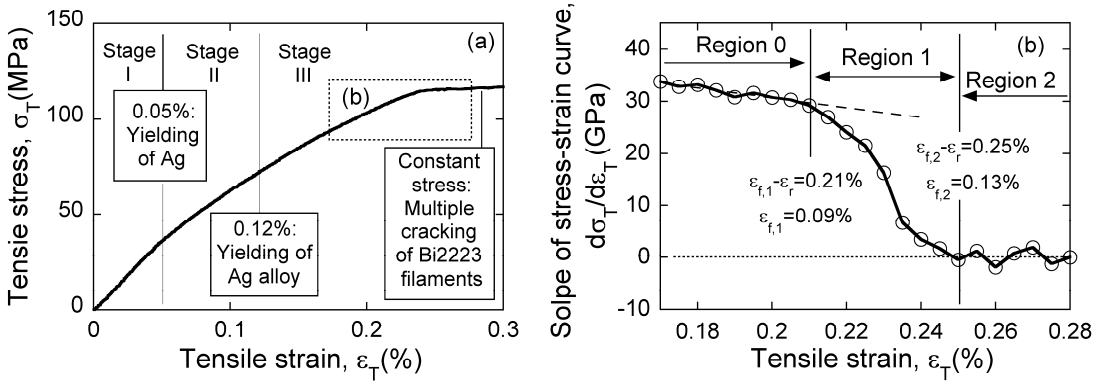

Fig.5

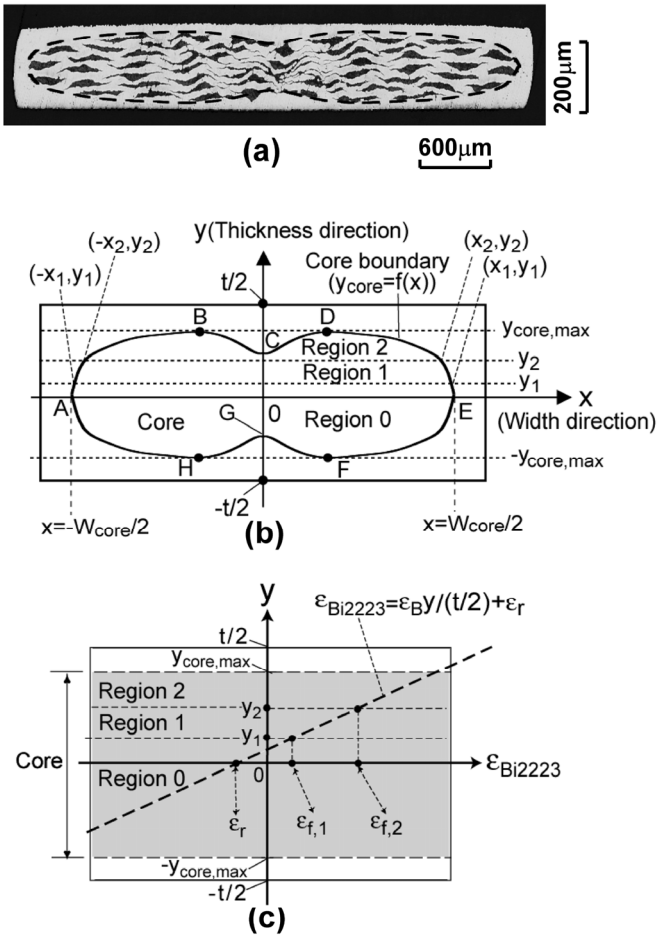

Fig.6

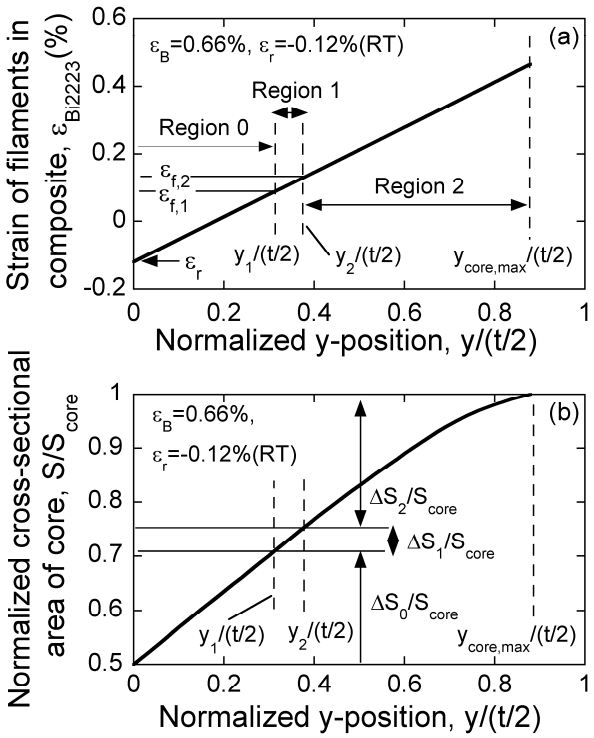

Fig.7

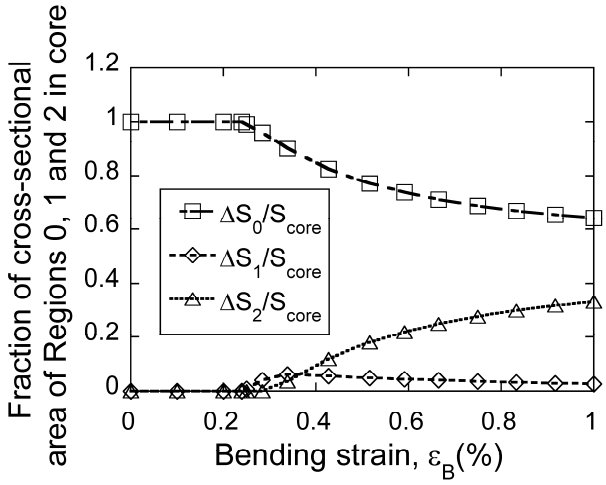

Fig.8

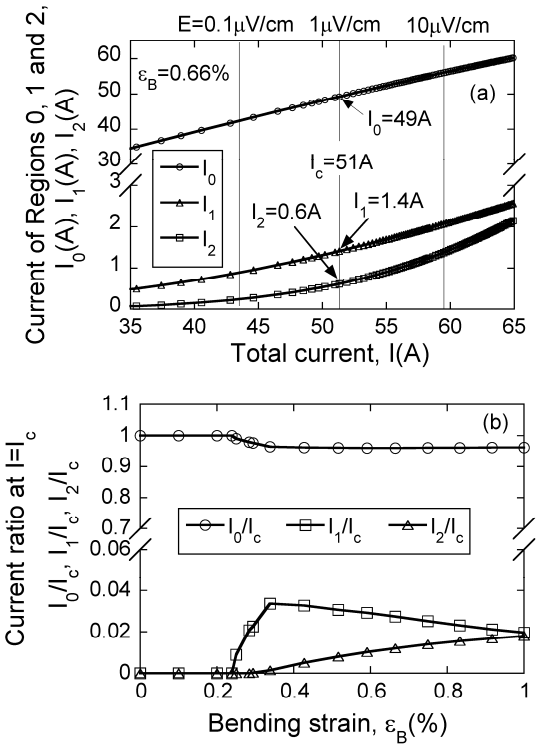

Fig.9

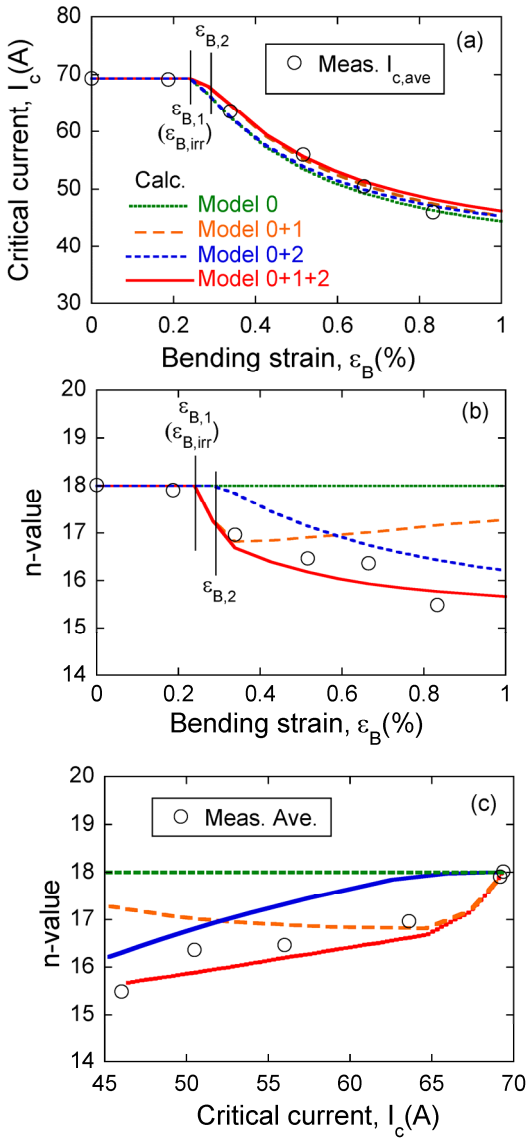

Fig.10